Coupled-channel analysis of collisional effects on HFS transitions in antiprotonic helium atoms

G.Ya. Korenman and S.N. Yudin
Institute of Nuclear Physics, Moscow State University, Moscow, Russia
e-mail: korenman@anna19.sinp.msu.ru

Abstract

Collisions of metastable antiprotonic helium with atoms of medium induce transitions between hyperfine structure sublevels as well as shifts and broadenings of the microwave M1 spectral lines. We consider these phenomena in the framework of a simple model with scalar and tensor interactions between $(\bar{p}\mathrm{He}^+)_{nL}$ and He atoms. S-matrix is obtained by solving coupled-channels equations involving 4 HFS sublevels ($F = L \pm 1/2$, $J = F \pm 1/2$) of the nL level and relative angular momenta up to $l = 5$ at the kinetic energy $E \lesssim 25$ K. The calculated spin-flip cross sections are less than elastic ones by four orders of value in the cases $\Delta F = \Delta J = \pm 1$ and $\Delta F = 0$, $\Delta J = \pm 1$, and by seven orders of value in the case $\Delta F = \pm 1$, $\Delta J = 0$ or $\Delta J = \pm 2$. The considered cross sections reveal a resonance behaviour at very low energy ($E \sim 1 \div 4$ K depending on the model parameters). At the density $N = 3 \times 10^{20}$ cm^{-3} and $T = 6$ K we obtain the relaxation time $\tau(FJ \to F'J') \geq 160$ ns, the frequency shift $\Delta\nu \simeq 80$ kHz and the frequency broadening $\gamma \lesssim 5.9$ MHz for M1 spectral lines of the favored transitions ($\Delta F = \pm 1$, $\Delta J = \pm 1$). The results are compatible with the recent experimental data obtained by a laser-microwave-laser resonance method. With the temperature rising up to 25 K the rate of relaxation $\lambda = 1/\tau$ as well as shift and broadening of the M1 microwave lines are lowered by a factor $1.5 \div 2$ reflecting the displacement of a mean kinetic energy from the region of resonance scattering.

1 Introduction

Up to 1991 it was generally accepted that antiprotons after entering a matter would very quickly annihilate via strong interaction with nuclei of matter. However in 1991 at KEK it was discovered [1] that antiprotons could really survive in the midst of the ordinary helium atoms for the time intervals at least of the same order of value as the lifetime of the muon. This phenomenon is explained by the formation of the specific metastable states, for which radiative and Auger transitions are strongly suppressed. Similar states for hadronic helium atoms were predicted a long time ago [2]. Internal structure of the $(\bar{p}\mathrm{He}^+)^*$ metastable states can be considered, roughly, as electron in the ground state and antiproton in the nL -state with $n \approx n_0 = \sqrt{M^*/m_e} \approx 38$, where M^* is a reduced mass of $(\bar{p} - \mathrm{He}^+)$ system. The angular momentum L should be sufficiently large to form a circular or nearly-circular state, i.e. $L \approx n - 1$.

If antiproton has "sat down" on a such orbit, it will experience only a delayed annihilation. Therefore the sequence of the phenomena after entering of the antiprotons in matter seems to be as follows. When the antiproton will be proved to be in the helium target it quickly loses its energy through the ionization. When the kinetic energy falls below the ionization energy of helium atom ($I = 24.6$ eV), the antiproton knocks out one of the electrons in a He atom by the Coulomb interaction and occupies the orbit that is close to the orbit of the knocked electron. The formed $(\bar{p}\mathrm{He}^+)^*$ atom should have an initial kinetic energy about 5 eV as a recoil energy and after a time shorter than a nanosecond it reaches the thermal equilibrium with the medium.

After thermalization the antiprotonic atom will be in one of the states accessible for it and will proceed to collide with the neutral atoms of helium. These collisions will change the initial populations of the states of the antiproton atoms and also other their properties, such as rates of transitions, shifts and broadenings of spectral lines. These changes were identified by the method of laser resonance spectroscopy so it is opened a new layer of interesting physics (see [3] and the references therein). In particular, the density shifts and broadenings of E1 spectral lines ($nL \to n'L' = L \pm 1$) were observed for laser-induced transitions. The model theoretical analysis [4] shows that qualitative peculiarities of the data are related to quantum effects at very low temperature and peculiar features of $(\bar{p}\mathrm{He}^+) - \mathrm{He}$ interaction. More sophisticated calculations with *ab initio* potential surface [5] give a quantitative agreement with the experimental data for a lot of E1 transitions.

Recently, the first data on hyperfine structure of the $(n, L) = (37, 35)$ state of the $(\bar{p}\mathrm{He}^+)$ were obtained by a laser-microwave-laser resonance method [6]. The central frequencies of microwave M1-transitions, $\nu^+_{HF}(F = L - 1/2, J = L \to L + 1/2, L + 1) = 12.89596(34)$ GHz and $\nu^-_{HF}(L - 1/2, L - 1 \to L + 1/2, L) = 12.92467(29)$ GHz, are in excellent agreement ($\lesssim 30$ ppm) with the recent calculations for the isolated $(\bar{p}\mathrm{He}^+)$ system [7]. The results suppose that the density shifts of the M1 spectral lines at the experimental conditions are very small and do not exceed the experimental accuracy (~ 300 kHz), in contrast with the $E1$ transitions. However the width of the lines ($\gamma \sim 5.3 \pm 0.7$ MHz) leaves room for a collisional broadening. One more consequence of the data is that the mean time of the collisional relaxation $\tau_c(F = L - 1/2 \to F' = L + 1/2) \gtrsim 140$ ns, the latter number being the observation time window.

As far as we know there is no published theoretical papers on collisional effects on HFS states of the $(\bar{p}\mathrm{He}^+)$ system, except for our short paper [8]. We consider the problems in the frame of a simple model of $(\bar{p}\mathrm{He}^+) - \mathrm{He}$ potential [4] extended to the tensor interaction. In this paper we investigate the complex of the mentioned questions by the coupled channel method.

2 Formalism and Model

The method of coupled channels consists in the solution of the finite system of coupled differential equations, which is obtained from the total Schroedinger equation by developing a total wave function into a restricted set of the basis channel states. The number of the equation in this system is defined by the number of different states of the antiprotonic atom included into consideration and by the number of different partial waves of relative motion of colliding atoms at the given kinetic energy. that is necessary to get the reasonable cross sections. We take into account only four states arising as a result of spitting of

nL level, due to the interaction of the orbit L with spins of electron and antiproton. Four levels of the antiprotonic atom that were included into coupled channel system are shown on Fig. 1. The wave functions of the states can be written in a good approximation as a vector coupling of corresponding orbital and spin angular momenta,

$$|nL, s_e(F)s_{\bar{p}} : JM\rangle = \left((\Phi_{nL}(\xi) \otimes |s_e\rangle)_F \otimes |s_{\bar{p}}\rangle\right)_{JM}, \tag{1}$$

where $\Phi_{nL}(\xi)$ is a space wave function of the $(\bar{p}\mathrm{He}^+)$ in the state with a principal quantum number n and orbital quantum number L, ξ is a set of inner coordinates of the system, $|s_e\rangle$ and $|s_{\bar{p}}\rangle$ are spin functions of electron and antiproton, $F = L \pm 1/2$ and $J = F \pm 1/2$ are intermediate and total angular momenta of the split substates ($\mathbf{F} = \mathbf{L} + \mathbf{s}_e$, $\mathbf{J} = \mathbf{F} + \mathbf{s}_{\bar{p}}$).

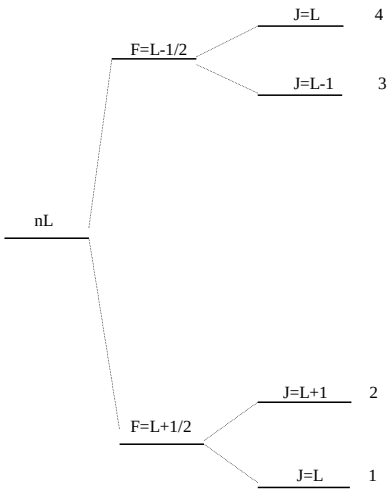

Figure 1: Hyperfine splitting of the $(\bar{p}\mathrm{He}^+)_{nL}$ level. The numbers on the right side from the sublevels are given for the short references to the states with definite F and J.

Further, it is necessary to fix the set of orbital momenta l of the relative motion of the antiprotonic and helium atoms. At the relative kinetic energy $E \leq 25$ K the wave number $k < 0.8$ a.u., and, with an effective radius of the model interaction (see below), we estimate $l_{\max} = 5$. We check also by the calculations with coupled channel equations that the contribution of the relative angular momenta $l > 5$ into the cross sections under consideration are negligible.

Now the channels will be defined by the quantum numbers of antiprotonic states, orbital angular momentum l and total angular momentum $j\,m$, where m is a projection of j on the quantization axes. Let us, for simplicity, to mark the total set of quantum numbers with c. Then the basis states can be written as follows

$$|c\rangle = \left(|nL, s_e(F)s_{\bar{p}} : J\rangle \otimes Y_l(\mathbf{n})\right)_{jm}, \tag{2}$$

where $\mathbf{n} = \mathbf{R}/R$ and $\mathbf{R}$ is a vector between centers of mass of the colliding subsystems. Total wave function of the $(\bar{p}\mathrm{He}^+) - \mathrm{He}$ system is expanded as a series in the basis states

$|c\rangle$ with the coefficients $\chi_c(R)/R$ depending on the interatomic distance R and satisfying to the system of coupled-channels equations

$$\left[\frac{d^2}{dR^2} + k_c^2 - \frac{l_c(l_c+1)}{R^2}\right]\chi_c(R) = 2M\sum V_{cc'}(R)\chi_{c'}(R) \tag{3}$$

where M is a reduced mass of colliding atoms, $k_c^2 = 2M[E-(\epsilon_c-\epsilon_i)]$, E is a relative kinetic energy in the input channel i, $\epsilon_c = \epsilon_{FJ}$ is the energy of the split level, and $V_{cc'}(R)$ is the matrix element of the interaction between channel states c and c'.

The central part of the interaction between the neutral exotic atom ($\bar{p}He^+$) and He atom contains a Van der Waals attraction ($\sim 1/R^6$) at a large distance and a strong repulsion at short distances [5, 9, 10]. Due to non-zero orbital angular momentum L of the antiprotonic helium, the total interaction could also include a tensor term that will couple the states with different projections Λ of the angular momentum L. In order to infer a form of the tensor interaction, let us consider a long-range dipole-dipole interaction between two atoms

$$\hat{V}_1 = [(\mathbf{D}\cdot\mathbf{d}) - 3(\mathbf{D}\cdot\mathbf{n})(\mathbf{d}\cdot\mathbf{n})]/R^3, \tag{4}$$

where $\mathbf{D}$ and $\mathbf{d}$ are dipole operators of the antiprotonic and ordinary atoms, respectively. Matrix elements of the interaction (4) between ground states of He atom disappear, however in the second-order perturbation theory it generates scalar and tensor terms of an effective Van der Waals interaction

$$\langle nL\Lambda|V(\xi,\mathbf{R})|nL\Lambda'\rangle = -\frac{1}{R^6}\left(C_6\delta_{\Lambda\Lambda'} + G_6\sum_\nu \langle L\Lambda' 2\nu|L\Lambda\rangle C^*_{2\nu}(\mathbf{n})\right), \tag{5}$$

where $C_{2\nu}(\mathbf{n}) = Y_{2\nu}(\mathbf{n})\sqrt{4\pi/5}$,

$$C_6 = \frac{2}{3}\sum_{m\gamma}\frac{|\langle m|\mathbf{d}|0\rangle|^2\,|\langle\gamma|\mathbf{D}|nL\Lambda\rangle|^2}{E_m - E_0 + \epsilon_\gamma - \epsilon_{nL}}, \tag{6}$$

$$G_6 = \frac{1}{2L+1}\sqrt{\frac{2}{3}}\sum_{\lambda\mu\nu\Lambda\Lambda' m\gamma}\langle 1\lambda 1\mu|2\nu\rangle\langle L\Lambda' 2\nu|L\Lambda\rangle\frac{|\langle m|\mathbf{d}|0\rangle|^2\langle nL\Lambda|D_\lambda|\gamma\rangle\langle\gamma|D_\mu|nL\Lambda'\rangle}{E_m - E_0 + \epsilon_\gamma - \epsilon_{nL}}. \tag{7}$$

The indexes $nL\Lambda, \gamma$ and $0, m$ refer to the states of exotic and ordinary atoms, respectively. At large n the density of the levels is rather large, therefore the main contributions into the sums over γ in (6) and (7) arise from the states with $|\epsilon_\gamma - \epsilon_{nL}| \ll |E_m - E_0|$. It allows to estimate the scalar and tensor Van der Waals constants in the closure approximation as

$$C_6 = \alpha\langle nL|\mathbf{D}^2|nL\rangle, \tag{8}$$

$$G_6 = \alpha\langle nL||\mathbf{D}^2 C_2(\mathbf{D}/D)||nL\rangle/\sqrt{2L+1}, \tag{9}$$

where $\alpha = 1.383$ a.u. is a static polarizability of He atom.

The simple radial dependence (5) of the interaction is valid only at long distances. For arbitrary distance we suppose

$$\langle nL\Lambda|V(\mathbf{R},\xi)|nL\Lambda'\rangle = V_0(R)\delta_{\Lambda\Lambda'} + V_2(R)\sum_\nu\langle L\Lambda' 2\nu|L\Lambda\rangle C^*_{2\nu}(\mathbf{n}), \tag{10}$$

where functions $V_0(R)$ and $V_2(R)$ could depend on the quantum numbers n, L. Radial dependence of the scalar term was taken in the form [4]

$$V_0(R) = -C_6 \cdot f(R), \qquad f(R) = (R^2 - r_c^2)/(R^2 + r_0^2)^4, \tag{11}$$

that has a repulsion at $R < r_c$, Van der Waals minimum at $R^2_{\min} = (r_0^2 + 4r_c^2)/3$ and the correct long-range asymptotic $V_0(R) \to -C_6/R^6$ at $R \to \infty$. Radial dependence of the tensor term at the large distance is similar, whereas at small distance it has to be $V_2(R) \sim R^2$. To satisfy these limits we suppose

$$V_2(R) = -G_6 \cdot f(R)[1 - \exp(-\eta R^2)], \tag{12}$$

with a large enough value of the parameter η (~ 10 a.u.) in order to avoid its influence at $R \gtrsim 1$ a.u.

For the calculations we use two sets of the parameters. The set A is based on the fitting [4] of the density shifts of E1-transitions ($nL \to n'L' = L \pm 1$), $C_6 = 2.82$, $r_c = 3.0$, $r_0 = 2.8$ (all values in atomic units). The second set (B) is estimated using the data of *ab initio* calculations of the potential energy surface [5, 9]. The repulsion radius, position and depth of the Van der Waals minimum of the potential $V_0(R)$ from Fig. 3 in [5] were used to obtain the values $C_6 = 3.35$, $r_c = 4.75$, $r_0 = 0.707$ (a.u.) for our form of the potential. For the both sets we adopt $G_6/C_6 = -0.37$ estimated by means of a single-particle model of ($\bar{p}\mathrm{He}^+$) with effective charges. A dependence of the parameters on n, L is rather weak and does not matter for our aims. On other hand, two sets of the parameters differ markedly, that allows to reveal general properties of characteristics to be considered. General dependencies of the scalar V_0 and tensor V_2 terms of the potential (10) on R are shown on Fig. 2.

The interaction (10) does not depend explicitly on the spin variables, therefore it can change the values of F and J only due to the vector coupling of the spins with the orbital angular momentum L. The matrix of the potential in the right part of equation (3) is reduced to the $3j$ and $6j$-symbols by the usual Racah algebra:

$$\begin{aligned}\langle nLFJ, l : j|V(\mathbf{R}, \xi)|nLF'J', l' : j\rangle = V_0(R)\delta_{FF'}\delta_{JJ'}\delta_{ll'} + V_2(R)(-1)^{j+F+F'+L+1}\cdot \\ \cdot\hat{L}\hat{F}\hat{F}'\hat{J}\hat{J}'\hat{l}\hat{l}' \begin{pmatrix} l' & 2 & l \\ 0 & 0 & 0 \end{pmatrix} \begin{Bmatrix} J & l & j \\ l' & J' & 2 \end{Bmatrix} \begin{Bmatrix} F & J & 1/2 \\ J' & F' & 2 \end{Bmatrix} \begin{Bmatrix} L & F & 1/2 \\ F' & L' & 2 \end{Bmatrix},\end{aligned} \tag{13}$$

where $\hat{a} \equiv \sqrt{2a+1}$.

With these potentials, we solve coupled channels equations including 4 HFS sublevels at fixed nL and relative angular momenta up to $l = 5$ at the kinetic energy $E \leq 25$ K and obtain S-matrix in the representation of quantum numbers F, J, l, j. Elastic and inelastic cross sections and rates of the collisional transitions between HFS states were calculated with the formulae:

$$\sigma(FJ \to F'J') = \frac{\pi}{k^2} \sum_{jll'} \frac{2j+1}{2J+1} \left|\delta_{ll'}\delta_{JJ'}\delta_{FF'} - \langle FJl|S^j|F'J'l'\rangle\right|^2, \tag{14}$$

$$\lambda(FJ \to F'J') = N\langle\langle v\sigma(FJ \to F'J')\rangle\rangle, \tag{15}$$

where N is an atomic density of the medium, and the double angular brackets in the right side of (15) stand for averaging over the thermal velocity distribution.

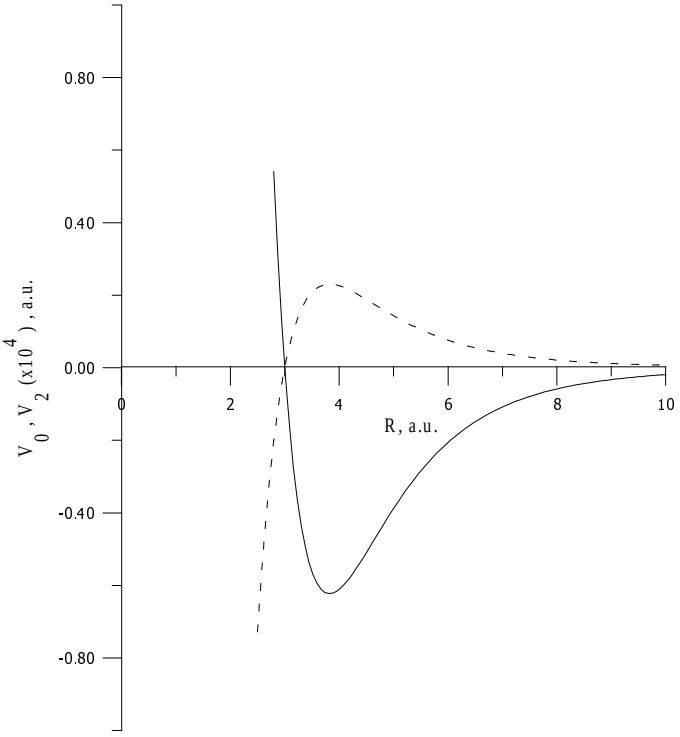

Figure 2: Radial dependence of the scalar $V_0(R)$ (solid line) and tensor $V_2(R)$ (dashed line) terms of the potential.

Collisional shifts and broadenings of the microwave M1 transitions ($FJ \to F'J'$) can be considered using a general theory of similar effects in atoms. For non-overlapping levels, Eq. (57.96) from [11] is relevant to our problem, and, with our notations of the quantum numbers, becomes

$$\gamma + \mathrm{i}\Delta = N\pi \sum_{ll'j_1j_2} (2j_1+1)(2j_2+1)(-1)^{l+l'} \begin{Bmatrix} j_1 & j_2 & 1 \\ J_2 & J_1 & l \end{Bmatrix} \begin{Bmatrix} j_1 & j_2 & 1 \\ J_2 & J_1 & l' \end{Bmatrix} \cdot \langle\langle vk^{-2}[\delta_{ll'} - \langle nLF_1J_1l'|S_I^{j_1}|nLF_1J_1l\rangle\langle nLF_2J_2l'|S_{II}^{j_2}|nLF_2J_2l\rangle^*]\rangle\rangle, \quad (16)$$

where S-matrix with the subscript I (II) corresponds to the collisions before (after) the radiative M1 transition $F_1J_1 \to F_2J_2$.

It should be noted that the averaging over the thermal velocity distribution in Eq. (16) has to be done in such way that S_I and S_{II} are taken at equal kinetic energies in the corresponding channels, i.e., at the total energies differed by the HFS splitting, because radiative transitions ($I \to II$) don't change kinetic energy. In the computational aspect, it means that for each kinetic energy E in the channel F_1, J_1 we have to solve

coupled-channel equations (3) four times, at the total energies $E + \epsilon(F_1 J_1) - \epsilon(F_2 J_2)$ for all four states $F_2 J_2$. In spite of the smallness of the splitting, it is comparable with the thermal energy at low temperature. Moreover, a presence of resonance scattering in the considered energy region (see next Section) can make the effect of the displacement of the total energies in the channels I and II to be drastically important for the calculations of the shift and broadening (16).

3 Results and discussions

The values of elastic and inelastic cross sections (14), rates of collisional transitions (15), shifts and broadenings (16) of the M1 spectral lines due to collisions of $(\bar{p}\mathrm{He}^+)$ with He atoms were calculated in this paper for all possible pairs of initial and final states $(FJ, F'J')$. Typical results of the calculations are shown on Figs. 3 - 6.

It should be noted that elastic cross sections are practically coincide for all four states $|FJ\rangle$ at the same kinetic energy in the corresponding channel, so they are indistinguishable on the figures. Much of the same is true for the pair of inelastic cross sections for the transitions with the spin-flip similarity, e.g., $\sigma(4 \to 2) \simeq \sigma(3 \to 1)$, $\sigma(4 \to 3) \simeq \sigma(2 \to 1)$. Therefore we show in Figs. 3 (a, b, c) elastic and inelastic cross section for the single initial state $(F = L - 1/2, J = F + 1/2)$ (number 4 on the energy diagram 1). Solid lines show the cross sections obtained with the set A of the parameters of the interaction potential, dashed lines show the similar cross-sections obtained with the set B of the parameters. Considering these results as well as the results for another initial states, we can see that elastic and inelastic cross sections have a similar energy dependence, but differ in magnitude by several orders of value. More definitely, inelastic cross sections corresponding to the single spin-flip (electron spin-flip $\Delta F = \Delta J = \pm 1$ or antiproton spin-flip $\Delta F = 0, \Delta J = \pm 1$) are less than elastic cross sections by four orders of value, whereas inelastic cross sections for the double, electron and antiproton, spin-flip ($\Delta F = \pm 1$, $\Delta J = 0$ or $\Delta J = \pm 2$) are less than elastic cross sections by seven orders of value.

Also, it is seen from Fig. 3 that the cross sections are essentially dependent on the parameters of the potential. So, an investigation of the elastic cross section can, in principle, shed light on the potential of interaction between antiprotonic and ordinary atoms. However, the most interesting feature of the cross sections on this figure is a pronounced maximum for all cross sections at a low energy (about 3 K for the set A of the parameters). This maximum is presented in all channels of the elastic and inelastic scattering and therefore should be due to the existence of resonances (quasistationary levels). Analysis of the results reveals the resonances in S, P and D-partial waves at the nearly equal energy ($\simeq$ 3 K). Appearance of these quasistationary states is due to the radial dependence of potential (see Fig. 2), which has a wide region of the attraction bounded by a repulsive barrier at $R = r_c$ and by a centrifugal barrier at large R. This part of the potential in principle could ensues the existence of quasistationary levels. A possible existence of the resonances as well as of bound states in the system in the $(\bar{p}\mathrm{He}^+)_{nL} - \mathrm{He}$ was discussed for the first time in the paper [4] with account for the scalar term $V_0(R)$ of the potential. Recently this prediction was confirmed in the calculations with an averaged *ab initio* potential [12]. It is of the interest that for the set B of the parameters of the potential the resonance is shifted to lesser energies and appears itself as the strong growth of the cross-section at lesser energies.

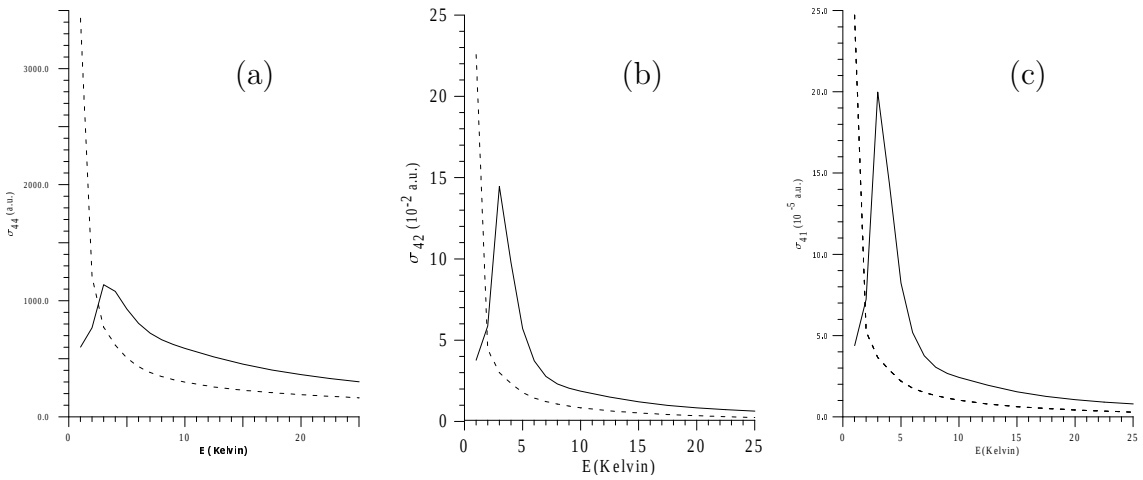

Figure 3: Cross sections of $(\bar{p}\mathrm{He}^+)_{nL} - \mathrm{He}$ collisions *vs.* c.m. kinetic energy: (a) elastic cross section σ_{44} for the initial HFS state $|4\rangle = |F = L - 1/2, J = F + 1/2\rangle$; (b) inelastic (de-excitation) cross section σ_{42} for the 'electron spin-flip' transition $4 \to 2$; (c) inelastic (de-excitation) cross section σ_{41} for the 'electron and antiproton spin-flip' transition $4 \to 1$. Solid and dashed lines refer to the sets A and B of the parameters of the potential.

The rates of transitions between HFS levels induced by collisions of the $(\bar{p}\mathrm{He}^+)_{nLFJ}$ with He atoms are connected with the cross sections by Eq. (15). Our results for the values $\lambda(i \to j)/N$ depending on temperature are shown on Fig. 4 for the transitions $4 \to 3$, $4 \to 2$ and $4 \to 1$. Solid and dashed lines are obtained with the sets A and B of the potential parameters, respectively. The rates of the single spin-flip transitions $4 \to 3$ and $4 \to 2$ are of the same order of value and rather large ($\sim N \cdot 10^{-14}\mathrm{cm}^3/\mathrm{s}$), whereas the rates of double spin-flip transitions are suppressed by three orders of value. For an interpretation of the experiment [6] the most interesting collisional transitions are those that change relative populations of upper (4 and 3) and lower (2 and 1) groups of the levels. We have noted in Introduction that it follows from the experiment that a relaxation time of the populations has to be of order or greater than a time gate between two laser pulses, i.e., 140 ns. This value should be compared with inverse rates of the transitions $4 \to 2$, $4 \to 1$, $3 \to 2$ and $3 \to 1$. According to our calculations, $\lambda(3 \to 1) \simeq \lambda(4 \to 2)$, whereas the rates of two other transitions are negligible. At the experimental conditions ($T = 6$ K, $N = 3 \times 10^{20}$ cm^{-3}) we obtain a collisional relaxation time $\tau_c = 1/\lambda(4 \to 2) = 160.5$ ns for the set A of the parameters, and $\tau_c = 325$ ns for the set B. The both values are greater than the mentioned time gate and, so, are compatible with the experiment.

It is seen from Fig. 4 that the resonances existing in the cross sections are not presented here in the form of maximum, but, due to averaging over the thermal motion, manifest itself as a reduction of the rates with increasing of the temperature: all considered rates $\lambda(FJ \to F'J')$ are reduced at least by factor 2 for the both sets (A and B) of the parameters when the temperature raises from $T = 3$ K to 25 K. In other words, the relaxation time of the populations of the HFS levels has to rise in the considered temperature region by factor about 2. This result may be especially interesting for the further experiments with HFS of the antiprotonic helium by the triple laser-microwave-laser resonance method, because a such temperature dependence of the relaxation time allows to

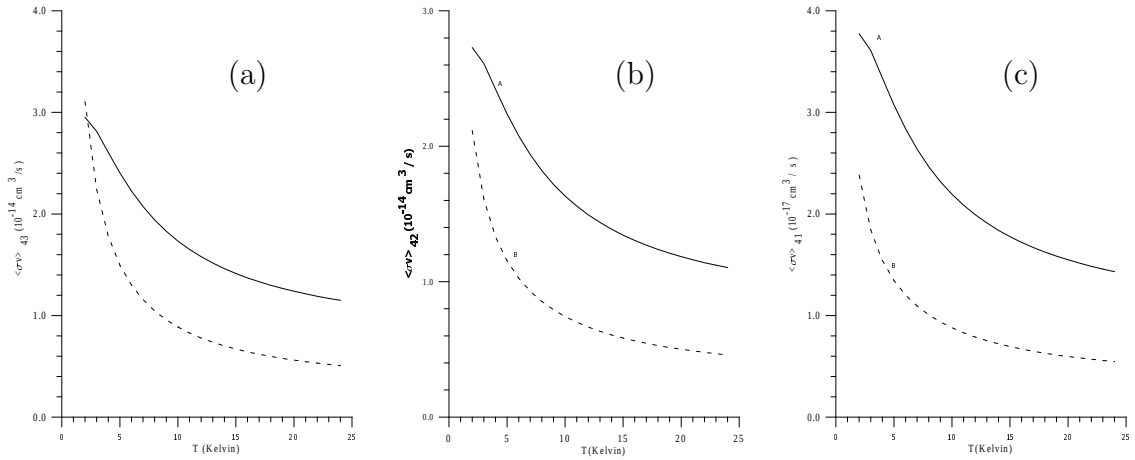

Figure 4: Temperature dependence of per-atom collisional transition rates $\lambda(i \to j)/N = \langle\langle\sigma(i \to j)v\rangle\rangle$; the figures (a), (b) and (c) are for the transitions $4 \to 3$, $4 \to 2$ and $4 \to 1$, respectively. The solid and dashed lines are obtained with the sets A and B of the parameters of the potential (11) - (12).

find more convenient conditions for the time gate between two laser pulses. Of course, we can not extrapolate the revealed T-dependence to higher temperature without further calculations. We took into account in these calculations the partial waves up to $l = 5$ that is enough in the considered region ($T < 25$ K). However, at higher temperature we can expect, from general point of view, that the main contribution to the rates far from the resonance region will give higher partial waves, and a number of essential partial waves will increase with the mean energy, therefore the rates could increase with temperature.

Per-atom density shift Δ/N and broadening Γ/N of the frequency of M1 spectral line $4 \to 2$ are shown on the Figs. 5 and 6, respectively. Left parts (a) of the figures display dependencies of the shift and broadening on kinetic energy (before averaging over Maxwell distribution), and right parts (b) show dependencies on temperature (with averaging over the Maxwell distribution). The solid and dashed lines correspond to the sets A and B of the parameters of the potential. The same curves could be referred to the $(3 \to 1)$ spectral line, because the results are indistinguishable in the scale of the figures.

A dependence of the shift of spectral lines on kinetic energy of the collision comes about as a result of interference of different partial waves, including resonant and non-resonant ones, as can be seen from the imaginary part of Eq. (16). Thus, it is understood some oscillations in the curves for the shift that one can see on the Fig. 5a. After averaging over Maxwell distribution on velocity, the oscillations disappear, and temperature dependence of the shift shows more smooth curves. Nevertheless, it is of some interest that the overall form of curves is defined by existence of resonance region at energy of several K.

On other side, broadening of the spectral lines reveals a resonance energy dependence (see Fig. 6a) similar to that one of the cross sections, because the real part of Eq. (16) contains incoherent contributions of different partial waves. After averaging over thermal motion we obtain the temperature dependence of the broadening (Fig. 6b), which is rather flat and decreases with temperature, as it recedes from the resonance region, similarly to the relaxation rates discussed above.

Considering shift and broadening at the experimental conditions ($T = 6$ K, $N =$

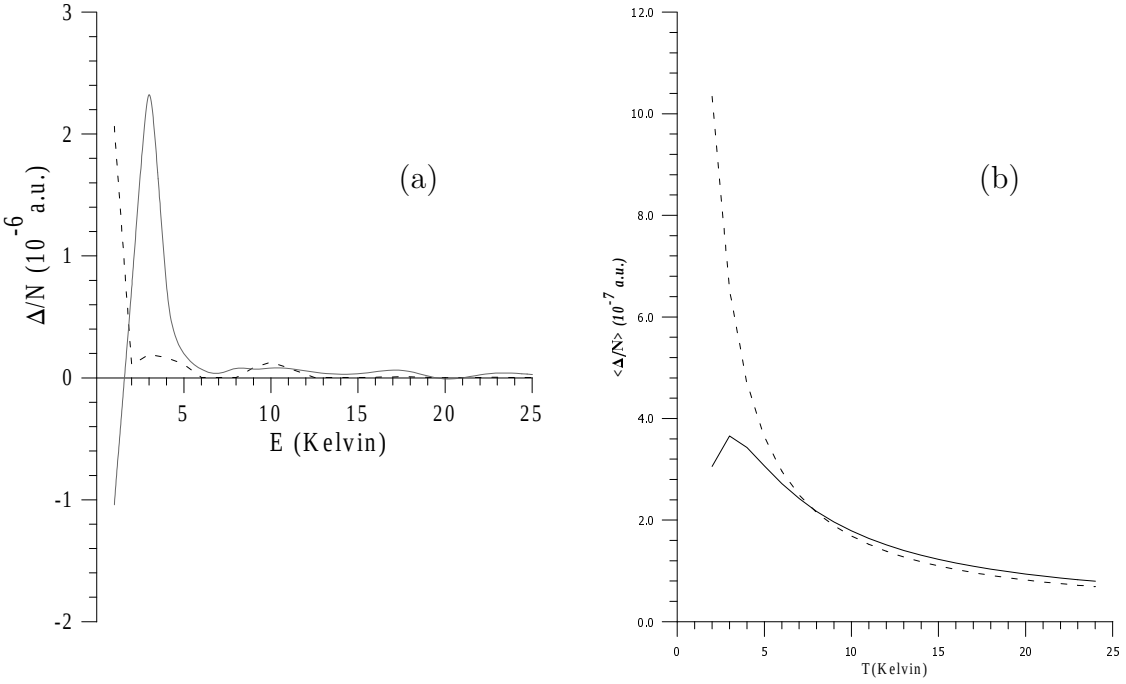

Figure 5: Per-atom density shift Δ/N of the M1 spectral line $4 \to 2$: (a) dependence on kinetic energy before averaging over Maxwell distribution, (b) dependence on temperature. The solid and dashed lines correspond to the sets A and B of the parameters of the potential. The curves for the shift of $(3 \to 1)$ spectral line are indistinguishable from the shown for the $4 \to 2$ spectral line.

3×10^{20} cm^{-3}), we have found the frequency shift of M1 spectral lines $\Delta\nu \simeq 79.5$ kHz for the favored transitions ($\Delta F = \pm 1$, $\Delta J = \pm 1$) with the set A, and rather close (86.6 kHz) with the set B of the potential parameters. This value is less than experimental accuracy ($\simeq$300 kHz) of the measured values $\nu^{\pm}_{HF}$, therefore the density shift could not be revealed in the experiment [6]. The calculated total broadening at the mentioned conditions for the same spectral lines is $\gamma = 5.92$ MHz and 2.66 MHz for the set A and B of the parameters, respectively. The both values are compatible with the experimental value of the broadening for the favored spectral lines (5.3 ± 0.7 MHz).

4 Conclusion

In this paper we have investigated a set of the effects of $(\bar{p}\mathrm{He}^+)_{nLFJ}-$He collisions on transitions between hyperfine-structure sublevels in the frame of coupled channel approach. We have taken into account four hyperfine-splitting states of the antiprotonic atom with quantum numbers n, L. With account for six states of relative orbital angular momentum, we have got twenty four coupled channels. A coupling between different channels was calculated in the model of Van der Waals forces with parameters obtained in two different approximations. Within this approach we have calculated the elastic and inelastic cross sections for all four states of the antiprotonic atom, as well as statistically averaged rates of transitions between HFS states, the energy and temperature dependencies of the

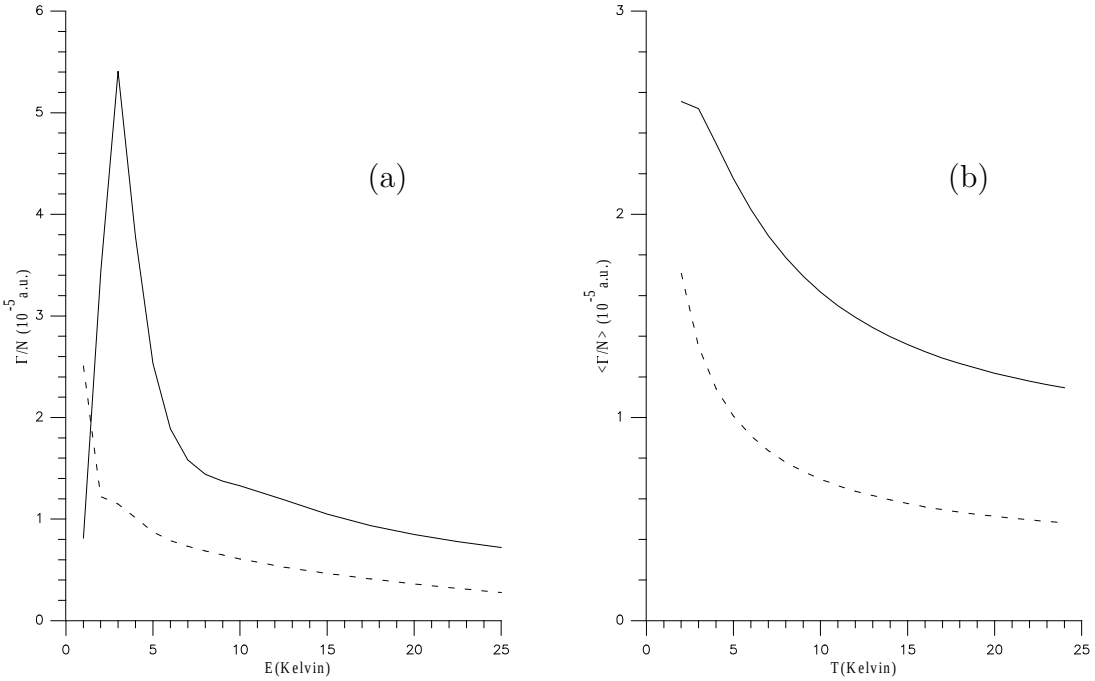

Figure 6: Per-atom density broadening Γ/N of the M1 spectral line $4 \to 2$: (a) dependence on kinetic energy before averaging over Maxwell distribution, (b) dependence on temperature. The solid and dashed lines correspond to the sets A and B of the parameters of the potential. The curves for the shift of $(3 \to 1)$ spectral line are indistinguishable from the shown for the $4 \to 2$ spectral line.

shifts and broadenings of the M1 spectral lines for different transitions. We consider that the main interest of our paper is in the consistent calculation of the whole set of collision characteristics of antiprotonic atoms with helium atoms of medium. For the cross sections in the elastic and inelastic channels we have observed the resonance region that is due to existence of quasistationary states in the chosen potential. Effects of the resonances should disappear after averaging over Maxwell distribution. This appears in the curves for the rates of the elastic and inelastic scattering. In this case one can guess about the existence of resonance region only by the decrease of rates at energies above 5 K. We have calculated the shifts and broadenings of M1 spectral lines as functions of energy and temperature. The shifts and broadenings is characterized with the strong maximum that is due to existence of resonances at the energies of the order 3-5 K. After averaging over the Maxwell distribution these maximum disappear that is quite naturally.

At the density and temperature corresponding to experimental conditions [6] ($N = 3 \times 10^{20}$ cm^{-3} and $T = 6$ K) we have obtained the relaxation times $\tau(FJ \to F'J') \geq 160$ ns, the frequency shifts of M1 spectral lines $\Delta\nu \simeq 80$ kHz for the favored transitions ($\Delta F = \pm 1$, $\Delta J = \pm 1$) and frequency broadening of the M1 spectral lines $\gamma \lesssim 5.9$ MHz. These results are compatible with the experimental data obtained by a laser-microwave-laser resonance method. With the temperature rising up to 25 K the rate of relaxation $\lambda = 1/\tau$ as well as shift and broadening of the M1 microwave lines are lowered by a factor $1.5 \div 2$ that may be useful a choice of conditions in further experiments.

Acknowledgements

This investigation was supported by Russian Foundation for Basic Research by the grant 03-02-16616. Authors thank to N.P. Yudin for the participation in the first stage of the work and for numerous discussions. One of the authors (G.K.) thanks to T. Yamazaki, R. Hayano and E. Widmann for attracting our interest to the considered problem, fruitful discussions and eliminating information on the experiment.

References

[1] M. Iwasaki, S.N. Nakamura, K. Shigaki, Y. Shimizu, H. Tamura, T. Ishikawa, R.S. Hayano, E. Takada, E. Widmann, H. Outa, M. Aoki, P. Kitching, T. Yamazaki, Phys. Rev. Lett. **67**, 1246 (1991).

[2] G.T. Condo, Phys.Lett, **9**, 65 (1964).

[3] T. Yamazaki, N. Morita, R.S. Hayano, E. Widmann and J. Eades, Physics Reports **366**, 183 (2002).

[4] G.Ya. Korenman, Hyperfine Interactions, **119**, 227 (1999).

[5] D. Bakalov, B. Jeziorski, T. Korona, K. Szalewich, Phys. Rev. Letters, **84**, 2350 (2000).

[6] E. Widmann, R.S. Hayano, T. Ishikawa, J. Sakuraguchi, T. Tasaki, H. Yamaguchi, J. Eades, M. Hori, H.A. Torii, B. Juhasz, D. Horvath, and T. Yamazaki, Phys. Rev. Letters **89**, 243402 (2002).

[7] D. Bakalov and V. Korobov, Phys. Rev. A **57**, 1662 (1998); V.Korobov and D.Bakalov, J. Phys. B: At. Mol. Opt. Phys. **34**, L519 (2001).

[8] G.Ya. Korenman, N.P. Yudin and S.N. Yudin, Nucl. Instruments and Methods in Physics Research, **B 214**, 94 (2004).

[9] J.E. Russel, Phys. Rev. A **1** (1970) 721.

[10] S. Sauge and P. Valiron, Chemical Physics, **265**, 47 (2001).

[11] G. Peach, Collisional broadening of spectral lines, in *Atomic, Molecular and Optical Physics Handbook,* ed. G.W.F. Drake, AIP Press, New York, 1996, Ch.57, p. 669.

[12] B.D. Obreshkov, D.D. Bakalov, B. Lepetit, and K. Szalevich, Phys. Rev. A **69** 042701 (2004).

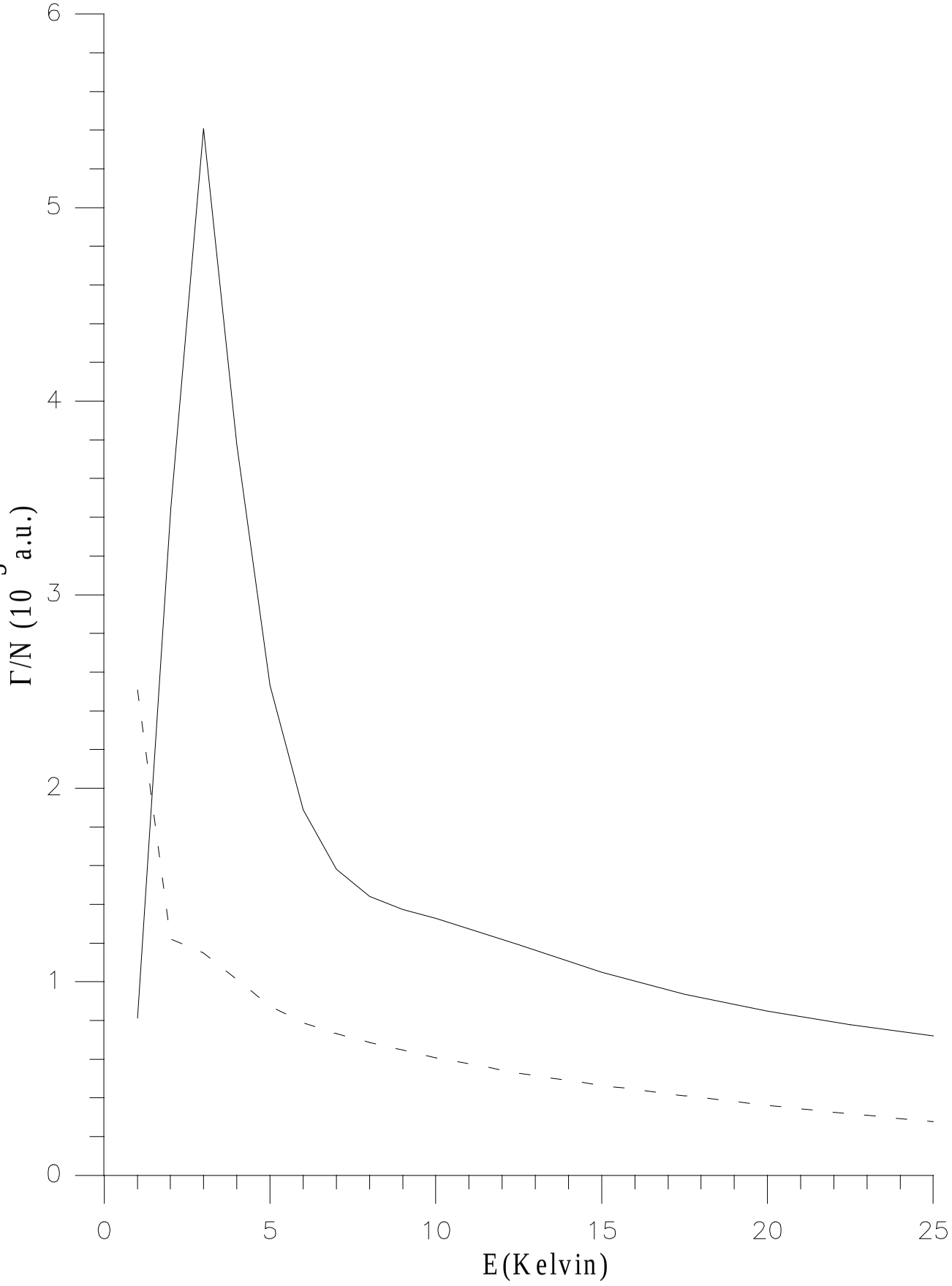
6
5
4
3
2
1
0
Γ/N (10^-5 a.u.)
0
5
10
15
20
25
E(Kelvin)

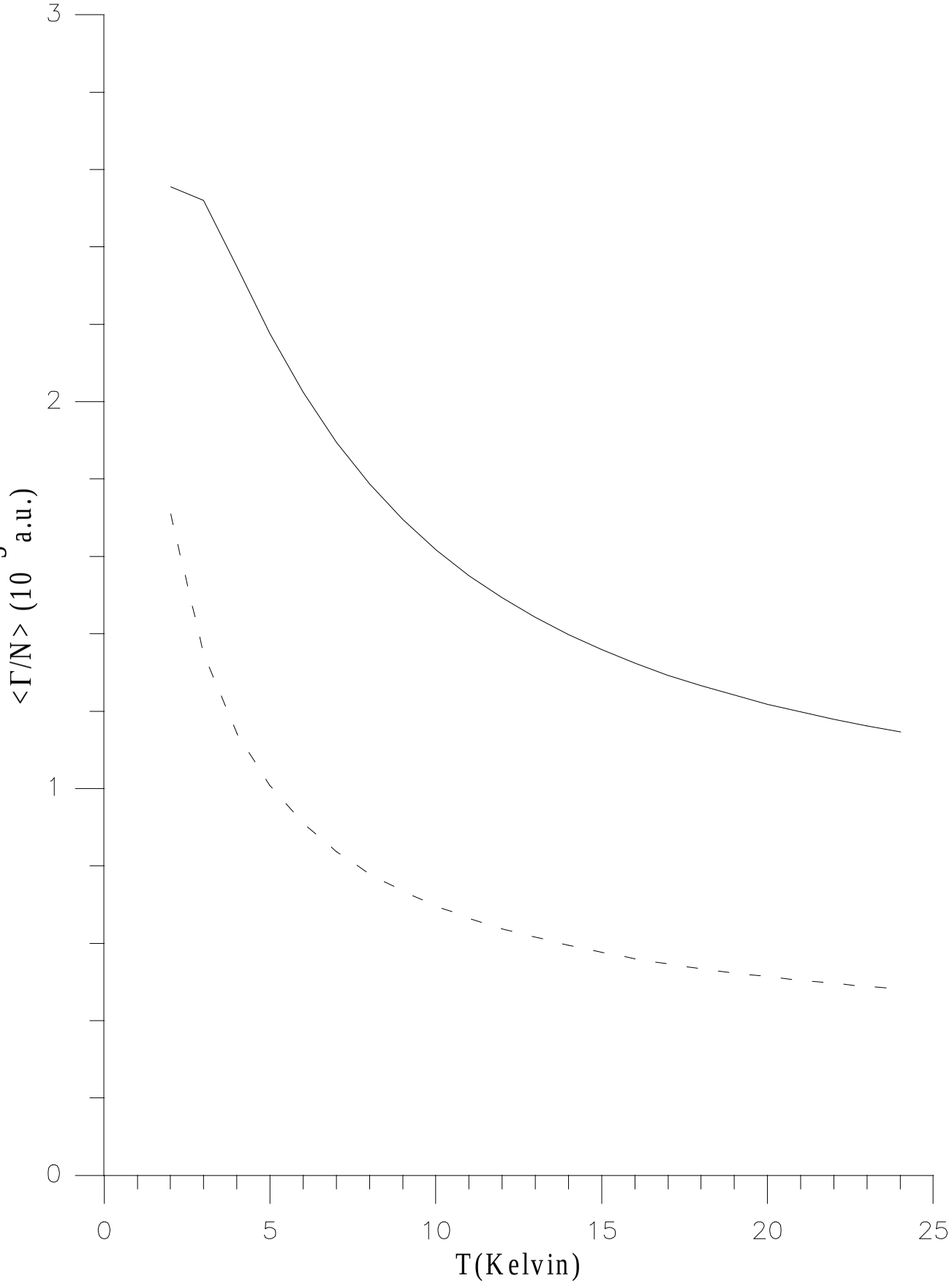
3
2
1
0
<Γ/N> (10^-5 a.u.)
0
5
10
15
20
25
T(Kelvin)